

# Crystal nucleation of highly screened charged colloids

Cite as: J. Chem. Phys. **157**, 154905 (2022); <https://doi.org/10.1063/5.0117867>

Submitted: 02 August 2022 • Accepted: 26 September 2022 • Accepted Manuscript Online: 26 September 2022 • Published Online: 20 October 2022

 Marjolein de Jager and  Laura Filion

## COLLECTIONS

Paper published as part of the special topic on [Nucleation: Current Understanding Approaching 150 Years After Gibbs](#)



View Online



Export Citation



CrossMark

## ARTICLES YOU MAY BE INTERESTED IN

[Guiding the self-assembly of colloidal diamond](#)

The Journal of Chemical Physics **157**, 154503 (2022); <https://doi.org/10.1063/5.0109377>

[Layering and capillary waves in the structure factor of liquid surfaces](#)

The Journal of Chemical Physics **157**, 154703 (2022); <https://doi.org/10.1063/5.0118252>

[Self-assembly and complex formation of amphiphilic star and bottle-brush block copolymers](#)

The Journal of Chemical Physics **157**, 154904 (2022); <https://doi.org/10.1063/5.0108479>



**The Journal of Chemical Physics**

**Special Topics** Open for Submissions

[Learn More](#)

# Crystal nucleation of highly screened charged colloids

Cite as: J. Chem. Phys. 157, 154905 (2022); doi: 10.1063/5.0117867

Submitted: 2 August 2022 • Accepted: 26 September 2022 •

Published Online: 20 October 2022



Marjolein de Jager<sup>a)</sup> and Laura Filion

## AFFILIATIONS

Soft Condensed Matter, Debye Institute of Nanomaterials Science, Utrecht University, Utrecht, Netherlands

**Note:** This paper is part of the JCP Special Topic on Nucleation: Current Understanding Approaching 150 Years After Gibbs.

<sup>a)</sup> Author to whom correspondence should be addressed: [m.e.dejager@uu.nl](mailto:m.e.dejager@uu.nl)

## ABSTRACT

We study the nucleation of nearly hard charged colloidal particles. We use Monte Carlo simulations in combination with free-energy calculations to accurately predict the phase diagrams of these particles and map them via the freezing density to hard spheres, then we use umbrella sampling to explore the nucleation process. Surprisingly, we find that even very small amounts of charge repulsion can have a significant effect on the phase behavior. Specifically, we find that phase boundaries and nucleation barriers are mostly dependent on the Debye screening length and that even screening lengths as small as 2% of the particle diameter are sufficient to show marked differences in both. This work demonstrates clearly that even mildly charged colloids are not effectively hard spheres.

Published under an exclusive license by AIP Publishing. <https://doi.org/10.1063/5.0117867>

## I. INTRODUCTION

Hard spheres are arguably the archetypal model system for studying colloidal self-assembly and have been instrumental in our understanding of, e.g., phase transitions,<sup>1–7</sup> glassy behavior,<sup>8–11</sup> and defects.<sup>12–16</sup> Experimentally, hard spheres are typically realized as colloidal particles suspended in a solvent. However, in such systems, the colloids nearly always carry surface charges and are generally decorated with surface ligands. This raises an important fundamental question: When can colloids be seen as hard spheres?

This question is particularly crucial when addressing crystal nucleation of hard spheres, where a long-standing issue is the large discrepancy between predicted and experimentally observed nucleation rates.<sup>1–3,6,17–24</sup> Since any induced repulsion between the particles will make the particles act as if they are slightly larger, a quantitative comparison to the true model requires a way to assign an effective packing fraction to the charged systems. From a historical perspective, the most common mapping involves assigning an effective diameter to the particles such that the freezing point matches that of hard spheres.<sup>1,13,18,25–32</sup> Within this mapping, it has been shown that for sufficiently large colloids, steric interactions due to surface ligands can indeed be accurately taken into account<sup>33</sup>—and this also holds for a simple short-ranged repulsion like the Weeks Chandler Andersen (WCA) potential.<sup>30</sup> It would be

tempting to, then, assume that this holds for screened charge interactions as well. Here, however, we will show that screened charge interactions clearly deviate from this pattern. We find that only extremely strongly screened charge interactions—ones where the screening length is at most a percent of the particle diameter—can be well approximated as hard sphere when it comes to nucleation.

## II. MODEL

We consider a system of  $N$  electrically like-charged hard spheres of diameter  $\sigma$  suspended in a solvent containing ions characterized by an inverse Debye screening length  $\kappa$  and Bjerrum length  $\lambda_B$ . Within Derjaguin–Landau–Verwey–Overbeek (DLVO) theory, the effective interaction potential is given by

$$\beta\phi(r) = \begin{cases} \beta\epsilon \frac{e^{-\kappa\sigma(r/\sigma-1)}}{r/\sigma} & \text{for } r \geq \sigma, \\ \infty & \text{for } r < \sigma, \end{cases} \quad (1)$$

with contact value  $\beta\epsilon = Z^2\lambda_B/\sigma(1 + \kappa\sigma/2)^2$ , where  $Z$  is the charge of the colloids in electron charge, and  $\beta = 1/k_B T$ , with  $k_B$  the

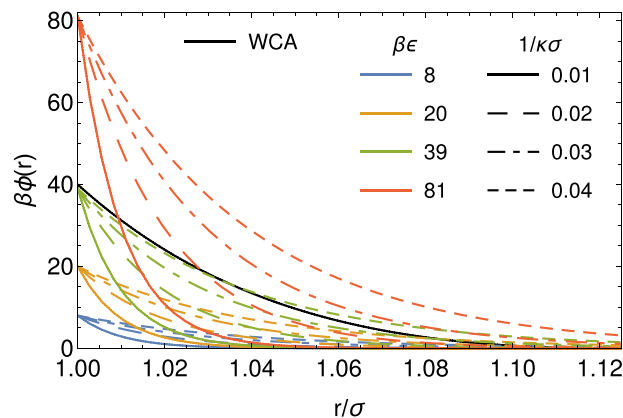


**FIG. 1.** Repulsive tail of the hard-core Yukawa potential for highly screened particles of diameter  $\sigma$  with contact value  $\beta\epsilon$  (colors) and screening length  $1/\kappa\sigma$  (dashing). The solid black line shows the WCA potential with  $\beta\epsilon = 40$ .

Boltzmann constant and  $T$  the temperature. Note that in the limit of zero charge ( $Z \rightarrow 0$ ) or infinite screening ( $\kappa\sigma \rightarrow \infty$ ), the repulsive hard-core Yukawa potential of Eq. (1) reduces to the hard-sphere potential. This system has been extensively studied using experiments, simulations, and theory, and the bulk phase behavior is extremely well understood.<sup>37–54</sup> Here, we focus on systems with short screening lengths, i.e., ranging from 1% to 4% of the particle diameter—similar to those often considered as hard experimentally.<sup>1,13,25,27,36,44,45,55</sup> For the contact values, we explore mainly  $\beta\epsilon = 8, 20, 39$ , and  $81$ , which allows us to compare with the phase diagrams of Ref. 43. An overview of the potentials is shown in Fig. 1. Additionally, in Fig. 1, we display the WCA potential with  $\beta\epsilon = 40$ , which was previously shown to accurately replicate the nucleation behavior of hard spheres.<sup>30</sup>

III. EFFECTIVE PHASE BOUNDARIES

We start by mapping the highly screened hard-core Yukawa particles to hard spheres using an effective hard-sphere diameter via  $\eta^{\text{eff}} = (\eta_F^{\text{HS}}/\eta_F)\eta$ , where  $\eta$  and  $\eta_F$  are the actual packing fraction and freezing packing fraction of the system, and  $\eta_F^{\text{HS}} = 0.492(1)$ <sup>34,35</sup> is the freezing packing fraction of hard spheres. To calculate the freezing and melting densities, we use free-energy calculations in combination with common-tangent constructions.<sup>34</sup> We first compute the equation of state of the fluid and face-centered cubic (FCC) crystal phase using Monte Carlo (MC) simulations in the  $NPT$ -ensemble with  $N = 2048$  particles. Additionally, to increase the accuracy of the equation of state, we use MC simulations in the  $NVT$ -ensemble combined with the virial equation, when the system does not “feel” the hard cores. In practice, this means that we only use the  $NVT$ -ensemble combined with the virial equation for systems with  $\beta\epsilon \geq 8$ . Next, we use thermodynamic integration of the equation of state to get the free energy as a function of the density.<sup>34</sup> For the fluid phase, we use the ideal gas as a reference system. For the FCC phase, we integrate from a reference density for which we computed the free energy using Einstein integration with finite-size corrections.<sup>34,35,56</sup>

A complete summary of all freezing and melting densities is given in Table I and the resulting effective melting packing fractions  $\eta_M^{\text{eff}}$  are shown Fig. 2(a). As expected, in the limit of zero charge ( $\beta\epsilon \rightarrow 0$ ), the melting density matches that of hard spheres. Surprisingly, however, this limit really requires nearly zero charge, with significant deviations appearing for contact values as low as  $\beta\epsilon = 1$ . For  $\beta\epsilon > 1.5$ ,  $\eta_M^{\text{eff}}$  is nearly unaffected by changing  $\beta\epsilon$ . As required, in the limit of infinite screening ( $1/\kappa\sigma \rightarrow 0$ ), the system reduces to hard spheres. However, as the screening length increases,  $\eta_M^{\text{eff}}$  steadily decreases. In the end,  $\eta_M^{\text{eff}}$  is comparable to  $\eta_M^{\text{HS}} = 0.543(1)$ <sup>34,35</sup> only for the

**TABLE I.** Freezing and melting packing fractions,  $\eta_F$  and  $\eta_M$ , of various systems of nearly hard spheres with contact value  $\beta\epsilon$  and screening length  $1/\kappa\sigma$ . The last two columns of the table give the effective hard-sphere melting packing fraction  $\eta_M^{\text{eff}} = (\eta_F^{\text{HS}}/\eta_F)\eta_M$ , with  $\eta_F^{\text{HS}} = 0.492(1)$ , and effective hard-sphere diameter  $\sigma_{\text{eff}}/\sigma = (\eta_F^{\text{HS}}/\eta_F)^{1/3}$ . Note that  $\eta_M^{\text{HS}} = 0.543(1)$ ,<sup>34,35</sup> and the error in  $\eta_F$  and  $\eta_M$  is  $\sim 0.001$ . To compare, the last two rows of the table give the values for the WCA system of Ref. 30 and experimental PMMA particles of Pusey and van Megen.<sup>36</sup>

$\beta\epsilon$	$1/\kappa\sigma$	$\eta_F$	$\eta_M$	$\eta_M^{\text{eff}}$	$\sigma_{\text{eff}}/\sigma$
8	0.01	0.458	0.505	0.542	1.024
20	0.01	0.446	0.491	0.542	1.033
39	0.01	0.437	0.482	0.542	1.040
81	0.01	0.429	0.472	0.541	1.047
8	0.02	0.432	0.473	0.538	1.044
20	0.02	0.410	0.449	0.538	1.063
39	0.02	0.395	0.432	0.538	1.076
81	0.02	0.380	0.415	0.538	1.090
8	0.03	0.412	0.447	0.534	1.061
20	0.03	0.381	0.414	0.534	1.089
39	0.03	0.361	0.393	0.535	1.108
81	0.03	0.341	0.371	0.535	1.130
8	0.04	0.396	0.426	0.530	1.075
20	0.04	0.358	0.386	0.530	1.111
39	0.04	0.334	0.360	0.531	1.138
81	0.04	0.310	0.334	0.531	1.167
0.5	0.04	0.476	0.523	0.541	1.011
1	0.04	0.472	0.512	0.534	1.014
1.5	0.04	0.463	0.500	0.531	1.021
2	0.04	0.453	0.489	0.530	1.028
3	0.04	0.439	0.472	0.529	1.039
4	0.04	0.426	0.458	0.529	1.049
5	0.04	0.415	0.447	0.529	1.058
6	0.04	0.408	0.439	0.529	1.065
7	0.04	0.403	0.434	0.530	1.069
8	0.04	0.396	0.426	0.530	1.075
WCA ( $\beta\epsilon = 40$ )		0.373	0.411	0.542	1.097
Pusey & v. Megen		0.407	0.442	0.534 <sup>a</sup>	1.065 <sup>a</sup>

<sup>a</sup> Note that Pusey and van Megen used  $\eta_F^{\text{HS}} = 0.494$ , whereas we use  $\eta_F^{\text{HS}} = 0.492$ . Here, we have corrected these values for this difference.

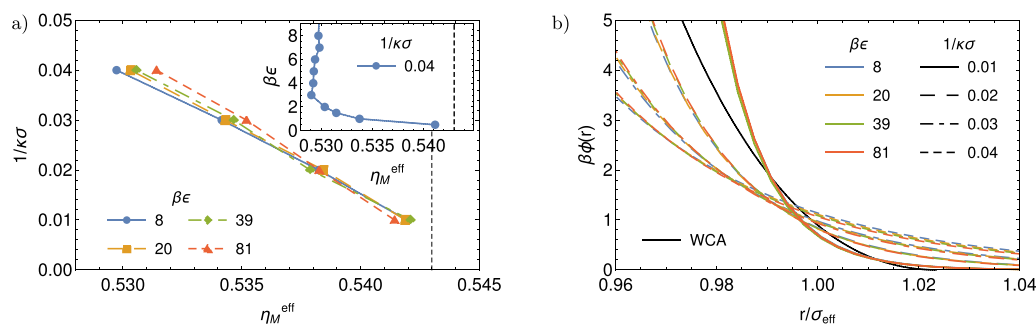


**FIG. 2.** (a) The effective hard-sphere melting packing fraction  $\eta_M^{\text{eff}} = (\eta_F^{\text{HS}}/\eta_F) \eta_M$ , as a function of the screening length  $1/\kappa\sigma$  for hard-core Yukawa particles with contact value  $\beta\epsilon$ . Additionally, the inset gives  $\eta_M^{\text{eff}}$  as a function of  $\beta\epsilon$  for  $1/\kappa\sigma = 0.04$ . The vertical dashed lines indicate  $\eta_M^{\text{HS}} = 0.543(1)$ .<sup>34,35</sup> The error in  $\eta_M^{\text{eff}}$  is  $\sim 0.001$ . (b) The corresponding interaction potentials around the effective hard-sphere diameter  $\sigma_{\text{eff}}$  plotted in units of  $\sigma_{\text{eff}}$  (see Table I). The solid black line shows the WCA potential with  $\beta\epsilon = 40$ .

strongest screening ( $1/\kappa\sigma = 0.01$ ) or the smallest contact value ( $\beta\epsilon = 0.5$ ). These results are particularly surprising when looking at a plot of the potentials (Fig. 1), as it is unclear from their appearance which ones are “hard enough” to map well onto hard spheres. Clearly, whether a specific potential will or will not map onto that of hard spheres cannot be seen simply by looking at the potential.

Nevertheless, we can explain why, for  $\beta\epsilon > 1.5$ ,  $\eta_M^{\text{eff}}$  should be unaffected by changing  $\beta\epsilon$ . For this, one needs to realize that, when the system does not feel the hard-core, the interaction potential of Eq. (1) reduces to the point Yukawa potential. In contrast to the phase behavior of hard-core Yukawa particles, the phase behavior of point Yukawa particles can be fully characterized by two parameters. Hence, when keeping  $1/\kappa\sigma$  fixed and resetting the length scale of the system using the freezing point,  $\beta\epsilon$  becomes obsolete. This becomes immediately apparent when looking at the interaction potential scaled by the effective diameter  $\sigma_{\text{eff}}/\sigma = (\eta_F^{\text{HS}}/\eta_F)^{1/3}$ , see Fig. 2(b). Here, we see that the potentials of equal  $1/\kappa\sigma$  all lie on top of each other. Note though that this only explains why a hard-core Yukawa system can be mapped onto another hard-core Yukawa system with a different contact value but the same screening length; it is still not trivial from the interaction potential whether a system will map well onto hard spheres or not.

#### IV. EFFECTIVE STRUCTURE

Next, we explore how well these potentials match the structure of the hard-sphere fluid, when mapped to the effective hard-sphere diameter. As we have seen that the effective behavior of the systems only depends on  $1/\kappa\sigma$ , here we focus on the structure of hard-core Yukawa particles with  $\beta\epsilon = 39$  and vary  $1/\kappa\sigma$ . Figure 3 shows the radial distribution function  $g(r)$  and the structure factor  $S(q)$  for these fluids at the freezing and melting packing fractions. Notice that all horizontal axes are scaled by the effective hard-sphere diameter and that this results in an excellent mapping of the  $g(r)$  and  $S(q)$ . The most significant differences between the structure of the hard spheres and the nearly hard spheres are the very slight broadening of the first peak of the  $g(r)$  and the mild

shrinking of the higher order peaks of the  $S(q)$ . These differences increase with increasing softness ( $1/\kappa\sigma$ ), essentially not existing when  $1/\kappa\sigma = 0.01$ .

#### V. NUCLEATION BARRIERS AND RATES

We now turn our attention to the nucleation behavior of these nearly hard particles. To study the crystal nucleation, we use MC simulations in the  $NPT$ -ensemble combined with umbrella sampling and measure the nucleation free-energy barriers. Following Refs. 22 and 30, we bias the simulation using the number of particles in the nucleus measured via the Ten Wolde order parameter<sup>57</sup> with cutoff values  $d_c = 0.7$  and  $\xi_c = 6$ , see the supplementary material. We use a fixed radial cutoff  $r_c$  to determine the nearest neighbors. It is chosen to be approximately the position of the first minimum of the radial distribution function for each state point.

We compute the nucleation barriers for the various hard-core Yukawa systems at a fixed effective packing fraction of the supersaturated fluid of  $\eta^* = 1.088\eta_F$ , which corresponds to hard spheres at a pressure of  $\beta P\sigma^3 = 17.0$ . The resulting nucleation barriers are shown in Fig. 4. For each system, we use  $N = 10976$ , and Table II contains all other necessary information per system. Additionally, Table II gives the interfacial free energy, critical nucleus size, and barrier height obtained from fitting the nucleation barriers (see the supplementary material). Based on our estimates, the error in the barrier height is no more than  $1k_B T$ . Looking at Fig. 4 and Table II, we see that, as expected and similar to  $\eta_M^{\text{eff}}$  in Fig. 1(b), the nucleation barriers are grouped together according to  $1/\kappa\sigma$ . Furthermore, we see that the systems with  $1/\kappa\sigma = 0.01$  map well to hard spheres and that increasing  $1/\kappa\sigma$ , i.e., increasing the softness of the particles, increases the height of the nucleation barrier. This is not entirely surprising, as the supersaturation, see Table II, decreases with increasing  $1/\kappa\sigma$ .

Next, we compute the nucleation rates for these systems. The methods are explained in the supplementary material. To calculate the attachment rate, we select 10 independent configurations from the umbrella simulations of the windows on top of the barrier and start 10 independent kinetic MC simulations from each

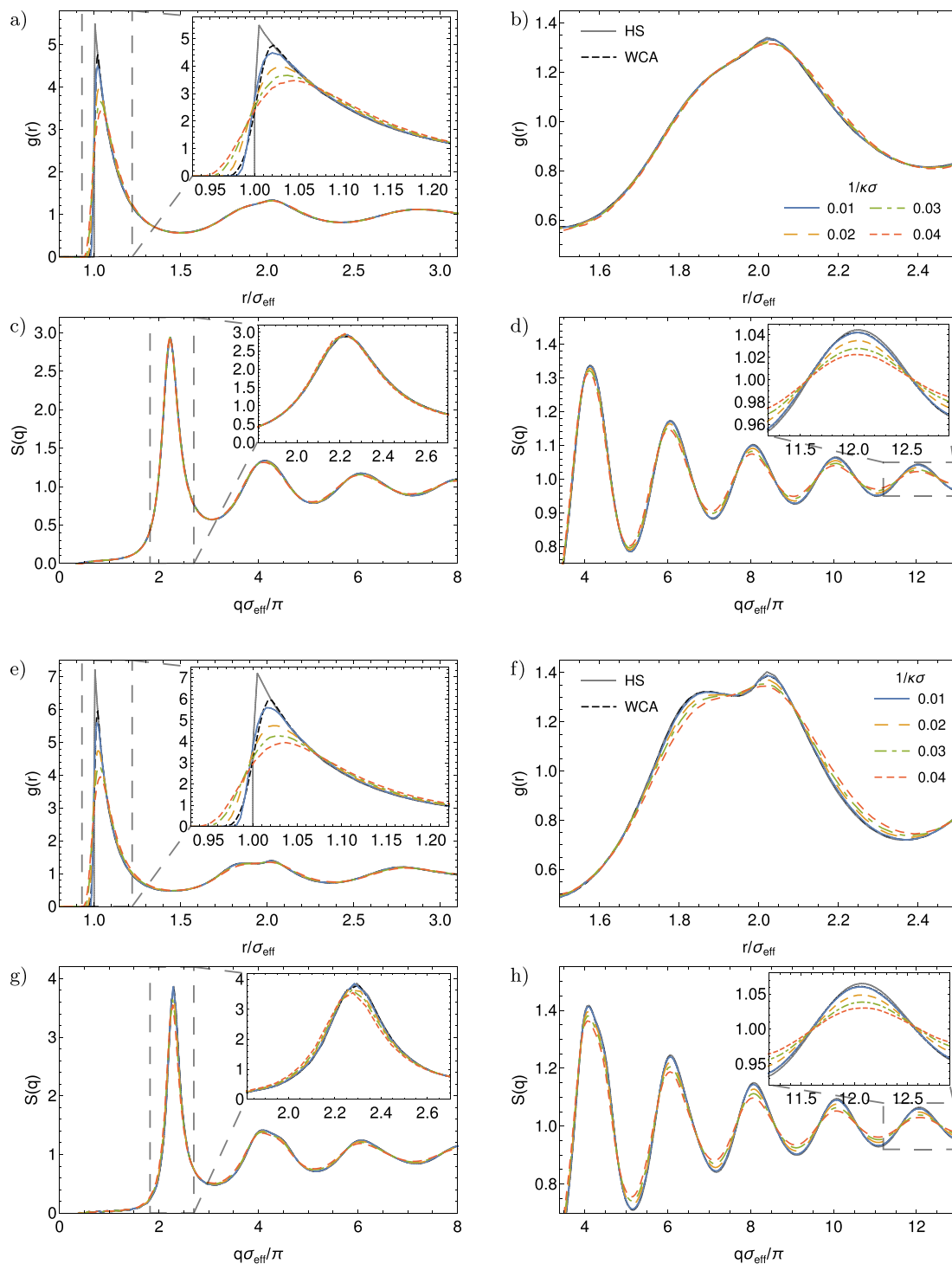


**FIG. 3.** The effective structure for a fluid of hard spheres (gray, solid), WCA particles with  $\beta\epsilon = 40$  (black, dashed), and hard-core Yukawa particles with  $\beta\epsilon = 39$  and varying screening length  $1/\kappa\sigma$  (colors, dashed). (e)–(f) is removed, please change the highlighted part of the caption to: (a)–(d) The results for the fluids studied at the freezing packing fraction, and (e)–(h) the fluids studied at the melting packing fraction. Here (a)–(b), (e)–(f) show the radial distribution function  $g(r)$ , where the insets of (a), (e) zoom in on the first peak of the  $g(r)$ , and (b), (f) show the second peak. The figures (c)–(d), (g)–(h) show the structure factor  $S(q)$ , where the insets of (c), (g) zoom in on the first peak of the  $S(q)$ , and (d), (h) show the second to sixth peak with the inset zooming in on the sixth peak. Note that all horizontal axes are scaled by the effective hard-sphere diameter  $\sigma_{\text{eff}}$ , see Table I.

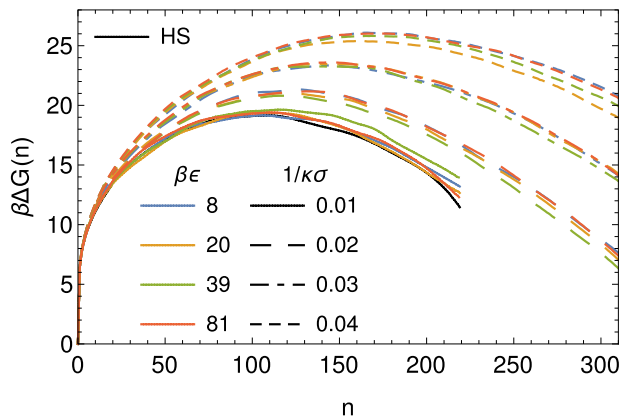


**FIG. 4.** Nucleation barriers of the FCC crystal of hard-core Yukawa particles with contact value  $\beta\epsilon$  (colors) and screening length  $1/\kappa\sigma$  (dashing) for a packing fraction of the supersaturated fluid of  $\eta^* = 1.088\eta_F$ . The corresponding hard-sphere barrier is shown by a black solid line. For more information, see Table II.

configuration. The resulting attachment and nucleation rates in terms of the long-time diffusion coefficient  $D_l$  are given in Table III. The error in the attachment rate is  $\sim 10\%$ . Combining this with the  $1k_B T$  error in the barrier height gives an error in the nucleation rate of approximately a factor 3. The nucleation rate found for the

**TABLE III.** Nucleation rate  $k$  in terms of the long-time diffusion coefficient  $D_l$  for a few of the systems of Table II. The third and fourth columns give the second derivative of the nucleation barrier and the attachment rate, both on top of the barrier, used for calculating  $k$ . The error in  $k$  is approximately a factor 3.

$\beta\epsilon$	$1/\kappa\sigma$	$\beta\Delta G''(n^*)$	$f_{n^*}/6D_l$	$k\sigma^5/6D_l$
Hard spheres		$-1.2 \times 10^{-3}$	$2.1 \times 10^3$	$1.5 \times 10^{-7}$
8	0.01	$-1.1 \times 10^{-3}$	$2.5 \times 10^3$	$1.5 \times 10^{-7}$
81	0.01	$-1.2 \times 10^{-3}$	$6.6 \times 10^3$	$3.1 \times 10^{-7}$
8	0.02	$-1.1 \times 10^{-3}$	$2.8 \times 10^3$	$2.1 \times 10^{-8}$
8	0.03	$-8.0 \times 10^{-4}$	$3.0 \times 10^3$	$2.5 \times 10^{-9}$
8	0.04	$-6.1 \times 10^{-4}$	$3.3 \times 10^3$	$1.7 \times 10^{-10}$
81	0.04	$-6.2 \times 10^{-4}$	$4.9 \times 10^3$	$1.7 \times 10^{-10}$

hard-spheres system agrees with the ones given in Refs. 3 and 22. Furthermore, notice that the nucleation rates of the systems with  $\beta\epsilon = 81$  agree within the error given with the corresponding system of  $\beta\epsilon = 8$ . This further confirms the accuracy of our calculations, considering that these systems are mapped onto each other when scaled with the effective hard-sphere diameter. As expected from the increasing barrier height, we see that the nucleation rate decreases with increasing  $1/\kappa\sigma$ . This is interesting, as this is in the opposite direction of the deviations between experiments and simulations for hard spheres. The “softer” particles studied in experiments have even

**TABLE II.** Interfacial free energy  $\beta\gamma\sigma^2$ , critical nucleus size  $n^*$ , and barrier height  $\beta\Delta G^*$  obtained from fitting to the nucleation barriers of Fig. 4. The third-fifth column give the cutoff radius  $r_c/\sigma$ , packing fraction  $\eta^*$  of the supersaturated fluid, and pressure  $\beta P\sigma^3$  used for the simulations, respectively. The sixth and seventh column give the density  $\rho_s\sigma^3$  of the solid phase and supersaturation  $\beta|\Delta\mu|$  used for fitting the barrier. The error in  $\beta\Delta G^*$  is no more than 1.

$\beta\epsilon$	$1/\kappa\sigma$	$r_c/\sigma$	$\eta^*$	$\beta P\sigma^3$	$\rho_s\sigma^3$	$\beta \Delta\mu $	$\beta\gamma\sigma^2$	$\beta\gamma/\rho_s^{2/3}$	$n^*$	$\beta\Delta G^*$
Hard spheres		1.40	0.5352	17.0	1.136	0.536	0.58	0.53	101	19.1
8	0.01	1.43	0.4985	16.0	1.053	0.531	0.53	0.52	103	19.2
20	0.01	1.45	0.4853	15.6	1.026	0.536	0.55	0.55	102	19.2
39	0.01	1.46	0.4757	15.2	1.005	0.530	0.53	0.53	108	19.6
81	0.01	1.47	0.4662	15.0	0.986	0.540	0.52	0.53	102	19.4
8	0.02	1.46	0.4699	15.4	0.983	0.494	0.57	0.57	116	21.2
20	0.02	1.49	0.4461	14.6	0.934	0.499	0.52	0.55	116	20.9
39	0.02	1.51	0.4298	14.1	0.901	0.502	0.52	0.56	114	20.7
81	0.02	1.53	0.4131	13.5	0.866	0.495	0.51	0.56	118	21.1
8	0.03	1.49	0.4477	15.1	0.927	0.452	0.52	0.55	142	23.2
20	0.03	1.52	0.4150	14.0	0.860	0.462	0.50	0.55	142	23.3
39	0.03	1.56	0.3932	13.2	0.815	0.458	0.49	0.57	137	23.2
81	0.03	1.58	0.3706	12.4	0.769	0.460	0.47	0.55	141	23.4
8	0.04	1.50	0.4304	15.1	0.882	0.411	0.50	0.54	172	25.8
20	0.04	1.56	0.3902	13.7	0.801	0.430	0.48	0.55	162	25.3
39	0.04	1.59	0.3630	12.6	0.746	0.424	0.45	0.54	168	25.7
81	0.04	1.63	0.3366	11.6	0.692	0.425	0.42	0.54	170	25.9



**TABLE IV.** Interfacial free energy  $\beta\gamma\sigma^2$ , critical nucleus size  $n^*$ , and barrier height  $\beta\Delta G^*$  obtained from fitting the nucleation barriers of Fig. 5. The third-fifth column give the cutoff radius  $r_c/\sigma$ , packing fraction  $\eta^*$  of the supersaturated fluid, and pressure  $\beta P\sigma^3$  used for the simulations, respectively. The sixth and seventh columns give the density  $\rho_s\sigma^3$  of the solid phase and supersaturation  $\beta|\Delta\mu|$  used for fitting the barrier. The error in  $\beta\Delta G^*$  is no more than 1.

$\beta\epsilon$	$1/\kappa\sigma$	$r_c/\sigma$	$\eta^*$	$\beta P\sigma^3$	$\rho_s\sigma^3$	$\beta \Delta\mu $	$\beta\gamma\sigma^2$	$\beta\gamma/\rho_s^{2/3}$	$n^*$	$\beta\Delta G^*$
Hard spheres		1.40	0.5352	17.0	1.136	0.536	0.58	0.53	101	19.1
8	0.01	1.43	0.4985	16.0	1.053	0.531	0.53	0.52	103	19.2
8	0.02	1.46	0.4724	15.8	0.988	0.532	0.51	0.51	93	18.0
8	0.03	1.48	0.4538	16.1	0.938	0.541	0.45	0.47	81	16.0
8	0.04	1.49	0.4399	16.7	0.900	0.541	0.41	0.44	69	14.8

faster rates than those predicted for purely hard spheres, meaning that the discrepancy between experiments and simulations cannot be explained by softness due to charge.

The question remains, is there a different way of mapping to hard spheres that leads to a better agreement for the nucleation rates? One option would be to map the entire coexistence region; however, for these systems, this would lead to lower  $\eta^*$  and thus to even higher barriers and slower nucleation rates. Another common practice is to compare nucleation rates at fixed  $\beta|\Delta\mu|$ . Notice that the systems with  $1/\kappa\sigma = 0.01$  in Table IV indeed have a  $\beta|\Delta\mu|$  comparable to that of the hard-sphere system. Here, we also compute the nucleation barriers for  $\beta\epsilon = 8$  with  $1/\kappa\sigma = 0.02, 0.03$ , and  $0.04$  at  $\beta|\Delta\mu| \approx 0.54$ . The necessary information for each system is given in Table IV, and Fig. 5 shows the resulting nucleation barriers. Contrary to the mapping at equal effective packing fraction, we now see that increasing  $1/\kappa\sigma$  decreases the height of the nucleation barrier, and again good agreement only occurs when  $1/\kappa\sigma = 0.01$ .

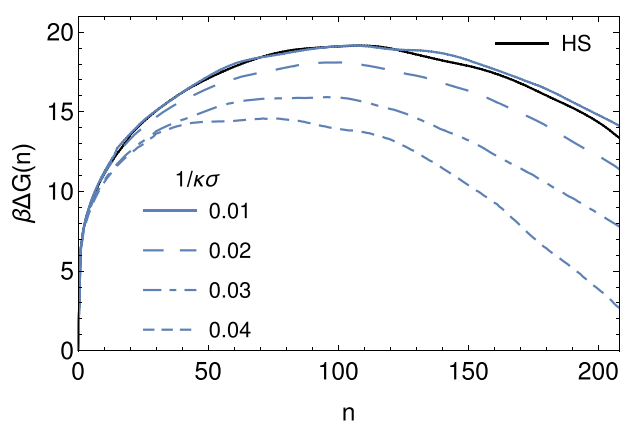


**FIG. 5.** Nucleation barriers of the FCC crystal of hard-core Yukawa particles with contact value  $\beta\epsilon = 8$  and screening length  $1/\kappa\sigma$  (dashing) for a supersaturation of  $\beta|\Delta\mu| \approx 0.54$ . The corresponding hard-sphere barrier is shown by black solid line. For more information, see Table IV.

## VI. CONCLUSIONS

In conclusion, we demonstrated that for highly screened particles, the phase behavior is incredibly sensitive to even very small amounts of charge repulsion. Specifically, we show that, when mapped to hard spheres via the freezing densities, the effective phase boundaries depend sensitively on the screening length, playing a measurable role even for screening lengths as low as  $1/\kappa\sigma \sim 0.02$ . Even though the effect of this on the effective structure of the system is barely perceivable, the nucleation rate is extremely sensitive to the change. This begs the question: When can experimental systems be considered hard spheres? The results here suggest that the answer is when the effective melting density matches that of hard spheres.

## SUPPLEMENTARY MATERIAL

In the [supplementary material](#), we provide a more in-depth description on the specific methods used for obtaining the nucleation barriers and rates. This includes a description of the Ten Wolde order parameter, umbrella sampling, fitting the nucleation barrier to classical nucleation theory, and calculating the nucleation rate.

## ACKNOWLEDGMENTS

We would like to thank Frank Smalenburg, Michiel Hermes, and Alfons van Blaaderen for many useful discussions. L.F. and M.d.J. acknowledge funding from the Vidi research program with Project No. VI.VIDI.192.102, which is financed by the Dutch Research Council (NWO).

## AUTHOR DECLARATIONS

### Conflict of Interest

The authors have no conflicts to disclose.

### Author Contributions

**Marjolein de Jager:** Conceptualization (supporting); Formal analysis (lead); Methodology (lead); Software (lead); Visualization (lead); Writing – original draft (lead); Writing – review & editing (equal).

**Laura Filion:** Conceptualization (lead); Funding acquisition (lead); Supervision (lead); Writing – original draft (supporting); Writing – review & editing (equal).

## DATA AVAILABILITY

An open data package containing the (analyzed) data and other means to reproduce the results of the simulations is available at: <https://doi.org/10.24416/UU01-8F4XK2> (Ref. 58).

## REFERENCES

- <sup>1</sup>J. L. Harland and W. Van Megen, *Phys. Rev. E* **55**, 3054 (1997).
- <sup>2</sup>U. Gasser, E. R. Weeks, A. Schofield, P. N. Pusey, and D. A. Weitz, *Science* **292**, 258 (2001).
- <sup>3</sup>S. Auer and D. Frenkel, *Nature* **409**, 1020 (2001).
- <sup>4</sup>A. Cacciuto, S. Auer, and D. Frenkel, *Nature* **428**, 404 (2004).
- <sup>5</sup>S. Auer and D. Frenkel, *Phys. Rev. Lett.* **91**, 015703 (2003).
- <sup>6</sup>S. Iacopini, T. Palberg, and H. J. Schöpe, *J. Chem. Phys.* **130**, 084502 (2009).
- <sup>7</sup>A. L. Thornework, J. L. Abbott, D. G. A. L. Aarts, and R. P. A. Dullens, *Phys. Rev. Lett.* **118**, 158001 (2017).
- <sup>8</sup>J. M. Gordon, J. H. Gibbs, and P. D. Fleming, *J. Chem. Phys.* **65**, 2771 (1976).
- <sup>9</sup>R. J. Speedy, *Mol. Phys.* **95**, 169 (1998).
- <sup>10</sup>E. Zaccarelli, S. M. Liddle, and W. C. K. Poon, *Soft Matter* **11**, 324 (2015).
- <sup>11</sup>A. L. Thornework, R. Roth, D. G. A. L. Aarts, and R. P. A. Dullens, *J. Chem. Phys.* **140**, 161106 (2014).
- <sup>12</sup>C. H. Bennett and B. J. Alder, *J. Chem. Phys.* **54**, 4796 (1971).
- <sup>13</sup>P. N. Pusey, W. Van Megen, P. Bartlett, B. J. Ackerson, J. G. Rarity, and S. M. Underwood, *Phys. Rev. Lett.* **63**, 2753 (1989).
- <sup>14</sup>S. Pronk and D. Frenkel, *J. Phys. Chem. B* **105**, 6722 (2001).
- <sup>15</sup>S. Pronk and D. Frenkel, *J. Chem. Phys.* **110**, 4589 (1999).
- <sup>16</sup>B. van der Meer, M. Dijkstra, and L. Filion, *J. Chem. Phys.* **146**, 244905 (2017).
- <sup>17</sup>C. Sinn, A. Heymann, A. Stipp, and T. Palberg, in *Trends Colloid Interface Science* (Springer, 2001), Vol. XV, p. 266.
- <sup>18</sup>K. Schätzel and B. J. Ackerson, *Phys. Rev. E* **48**, 3766 (1993).
- <sup>19</sup>S. Auer and D. Frenkel, *J. Chem. Phys.* **120**, 3015 (2004).
- <sup>20</sup>S. Auer and D. Frenkel, *Adv. Comput. Simul.* **173**, 149 (2005).
- <sup>21</sup>E. Zaccarelli, C. Valeriani, E. Sanz, W. C. K. Poon, M. E. Cates, and P. N. Pusey, *Phys. Rev. Lett.* **103**, 135704 (2009).
- <sup>22</sup>L. Filion, M. Hermes, R. Ni, and M. Dijkstra, *J. Chem. Phys.* **133**, 244115 (2010).
- <sup>23</sup>T. Schilling, S. Dorosz, H. J. Schöpe, and G. Opletal, *J. Phys.: Condens. Matter* **23**, 194120 (2011).
- <sup>24</sup>W. Wöhler and T. Schilling, *Phys. Rev. Lett.* **128**, 238001 (2022).
- <sup>25</sup>P. N. Pusey and W. van Megen, *Phys. Rev. Lett.* **59**, 2083 (1987).
- <sup>26</sup>S. M. Underwood, J. R. Taylor, and W. Van Megen, *Langmuir* **10**, 3550 (1994).
- <sup>27</sup>T. Palberg, *J. Phys.: Condens. Matter* **11**, R323 (1999).
- <sup>28</sup>C. P. Royall, W. C. K. Poon, and E. R. Weeks, *Soft Matter* **9**, 17 (2013).
- <sup>29</sup>T. Kawasaki and H. Tanaka, *Proc. Natl. Acad. Sci. U. S. A.* **107**, 14036 (2010).
- <sup>30</sup>L. Filion, R. Ni, D. Frenkel, and M. Dijkstra, *J. Chem. Phys.* **134**, 134901 (2011).
- <sup>31</sup>J. Russo, A. C. Maggs, D. Bonn, and H. Tanaka, *Soft Matter* **9**, 7369 (2013).
- <sup>32</sup>G. Fiorucci, G. M. Coli, J. T. Padding, and M. Dijkstra, *J. Chem. Phys.* **152**, 064903 (2020).
- <sup>33</sup>S. Auer, W. Poon, and D. Frenkel, *Phys. Rev. E* **67**, 020401 (2003).
- <sup>34</sup>D. Frenkel and B. Smit, *Understanding Molecular Simulation: From Algorithms to Applications*, 2nd ed. (Academic Press, San Diego, 2002).
- <sup>35</sup>J. M. Polson, E. Trizac, S. Pronk, and D. Frenkel, *J. Chem. Phys.* **112**, 5339 (2000).
- <sup>36</sup>P. N. Pusey and W. Van Megen, *Nature* **320**, 340 (1986).
- <sup>37</sup>S. Alexander, P. M. Chaikin, P. Grant, G. J. Morales, P. Pincus, and D. Hone, *J. Chem. Phys.* **80**, 5776 (1984).
- <sup>38</sup>K. Kremer, M. O. Robbins, and G. S. Grest, *Phys. Rev. Lett.* **57**, 2694 (1986).
- <sup>39</sup>M. O. Robbins, K. Kremer, and G. S. Grest, *J. Chem. Phys.* **88**, 3286 (1988).
- <sup>40</sup>Y. Monovoukas and A. P. Gast, *J. Colloid Interface Sci.* **128**, 533 (1989).
- <sup>41</sup>E. B. Sirota, H. D. Ou-Yang, S. K. Sinha, P. M. Chaikin, J. D. Axe, and Y. Fujii, *Phys. Rev. Lett.* **62**, 1524 (1989).
- <sup>42</sup>S. Hamaguchi, R. T. Farouki, and D. H. E. Dubin, *Phys. Rev. E* **56**, 4671 (1997).
- <sup>43</sup>A.-P. Hynninen and M. Dijkstra, *Phys. Rev. E* **68**, 021407 (2003).
- <sup>44</sup>A. Yethiraj and A. van Blaaderen, *Nature* **421**, 513 (2003).
- <sup>45</sup>C. P. Royall, M. E. Leunissen, and A. van Blaaderen, *J. Phys.: Condens. Matter* **15**, S3581 (2003).
- <sup>46</sup>M. F. Hsu, E. R. Dufresne, and D. A. Weitz, *Langmuir* **21**, 4881 (2005).
- <sup>47</sup>C. P. Royall, M. E. Leunissen, A.-P. Hynninen, M. Dijkstra, and A. van Blaaderen, *J. Chem. Phys.* **124**, 244706 (2006).
- <sup>48</sup>D. El Masri, P. van Oostrum, F. Smalenburg, T. Vissers, A. Imhof, M. Dijkstra, and A. van Blaaderen, *Soft Matter* **7**, 3462 (2011).
- <sup>49</sup>F. Smalenburg, N. Boon, M. Kater, M. Dijkstra, and R. van Roij, *J. Chem. Phys.* **134**, 074505 (2011).
- <sup>50</sup>T. Kanai, N. Boon, P. J. Lu, E. Sloutskin, A. B. Schofield, F. Smalenburg, R. van Roij, M. Dijkstra, D. A. Weitz *et al.*, *Phys. Rev. E* **91**, 030301 (2015).
- <sup>51</sup>S. Arai and H. Tanaka, *Nat. Phys.* **13**, 503 (2017).
- <sup>52</sup>M. Chaudhuri, E. Allahyarov, H. Löwen, S. U. Egelhaaf, and D. A. Weitz, *Phys. Rev. Lett.* **119**, 128001 (2017).
- <sup>53</sup>K. van Gruijthuisen, M. Obiols-Rabasa, M. Heinen, G. Nägele, and A. Stradner, *Langmuir* **29**, 11199 (2013).
- <sup>54</sup>T. E. Kodger, R. E. Guerra, and J. Sprakel, *Sci. Rep.* **5**, 14635 (2015).
- <sup>55</sup>M. Leunissen, Ph.D. thesis, 2007.
- <sup>56</sup>D. Frenkel and A. J. C. Ladd, *J. Chem. Phys.* **81**, 3188 (1984).
- <sup>57</sup>P.-R. ten Wolde, M. J. Ruiz-Montero, and D. Frenkel, *Faraday Discuss.* **104**, 93 (1996).
- <sup>58</sup>M. de Jager (2022). “Crystal nucleation of highly-screened charged colloids,” Utrecht University.